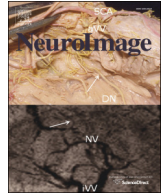




Contents lists available at ScienceDirect

NeuroImage

journal homepage: [www.elsevier.com/locate/ynimg](http://www.elsevier.com/locate/ynimg)

## Q1 Fast and powerful heritability inference for family-based neuroimaging studies

Q3 Q2 H. Ganjgahi <sup>a</sup>, A.M. Winkler <sup>b,c</sup>, D.C. Glahn <sup>c,d</sup>, J. Blangero <sup>e</sup>, P. Kochunov <sup>f</sup>, T.E. Nichols <sup>a,b,g,1</sup>

4 <sup>a</sup> Department of Statistics, The University of Warwick, Coventry, UK

5 <sup>b</sup> Centre for Functional MRI of the Brain, University of Oxford, Oxford, UK

6 <sup>c</sup> Department of Psychiatry, Yale University School of Medicine, New Haven, USA

7 <sup>d</sup> Olin Neuropsychiatry Research Center, Institute of Living, Hartford Hospital, Hartford, CT, USA

8 <sup>e</sup> Department of Genetics, Texas Biomedical Research Institute, San Antonio, TX, USA

9 <sup>f</sup> Maryland Psychiatric Research Center, Department of Psychiatry, University of Maryland School of Medicine, Baltimore, MD, USA

10 <sup>g</sup> WMG, The University of Warwick, Coventry, UK

### 1 1 A R T I C L E I N F O

#### 12 Article history:

13 Received 19 December 2014

14 Accepted 3 March 2015

15 Available online xxx

#### 16 Keywords:

17 Heritability

18 Permutation test

19 Multiple testing problem

### A B S T R A C T

Heritability estimation has become an important tool for imaging genetics studies. The large number of voxel- and vertex-wise measurements in imaging genetics studies presents a challenge both in terms of computational intensity and the need to account for elevated false positive risk because of the multiple testing problem. There is a gap in existing tools, as standard neuroimaging software cannot estimate heritability, and yet standard quantitative genetics tools cannot provide essential neuroimaging inferences, like family-wise error corrected voxel-wise or cluster-wise P-values. Moreover, available heritability tools rely on P-values that can be inaccurate with usual parametric inference methods.

In this work we develop fast estimation and inference procedures for voxel-wise heritability, drawing on recent methodological results that simplify heritability likelihood computations (Blangero et al., 2013). We review the family of score and Wald tests and propose novel inference methods based on explained sum of squares of an auxiliary linear model. To address problems with inaccuracies with the standard results used to find P-values, we propose four different permutation schemes to allow semi-parametric inference (parametric likelihood-based estimation, non-parametric sampling distribution). In total, we evaluate 5 different significance tests for heritability, with either asymptotic parametric or permutation-based P-value computations. We identify a number of tests that are both computationally efficient and powerful, making them ideal candidates for heritability studies in the massive data setting. We illustrate our method on fractional anisotropy measures in 859 subjects from the Genetics of Brain Structure study.

© 2015 Published by Elsevier Inc.

37

38

40

### 42 Introduction

Q5 Combining neuroimaging data with genetic analyses is an increasingly active area of research aimed at improving our understanding of the genetic and environmental control over brain structure and function in health and illness (see, e.g., Glahn et al., 2007). The foundation of any genetic analysis is establishing that a trait is heritable, that is, that a substantial fraction of its variability can be explained by genetic factors. Significant and reproducible heritability has been established for many neuroimaging traits assessing brain structure and function, including, for instance, location and strength of task-related brain activation (Blokland et al., 2008; Koten et al., 2009; Matthews et al., 2007; Polk et al., 2007), white matter integrity (Kochunov et al., 2014; Jahanshad

et al., 2013; Brouwer et al., 2010; Chiang et al., 2009, 2011; Kochunov et al., 2010), cortical and subcortical volumes, cortical thickness and density (Winkler et al., 2010; Rimol et al., 2010; Kochunov et al., 2011a, b; Kremen et al., 2010; den Braber et al., 2013).

Variance component models are the best-practice approach for deriving heritability estimates based on familial data (Almasy and Blangero, 1998; Blangero and Almasy, 1997; Amos, 1994; Hopper and Mathews, 1982), for allowing great flexibility in modeling of genetic additive and dominance effects, as well as common and unique environmental influences. The model also allows the inclusion of additional terms that allow linkage analysis, yet remaining relatively simple and requiring the estimation of only a few parameters. Estimation of parameters typically uses maximum likelihood under the assumption that the additive error follows a multivariate normal distribution. The iterative optimization of the likelihood function requires computationally intensive procedures, that are prone to convergence failures, something particularly problematic when fitting data at every voxel/element.

E-mail address: [t.e.nichols@warwick.ac.uk](mailto:t.e.nichols@warwick.ac.uk) (T.E. Nichols).

<sup>1</sup> Fax +44 24765 24532.

Typically a likelihood ratio test (LRT) is used for heritability hypothesis testing. As the null hypothesis value is on the boundary of the parameter space, the asymptotic distribution of LRT is not  $\chi^2$  with 1 degree of freedom (DF), but rather approximately as a 50:50 mixture of  $\chi^2$  distributions with 1 and 0 DF, where a 0 DF  $\chi^2$  is a point mass at 0 (Chernoff, 1954; Self and Liang, 1987; Stram and Lee, 1994; Dominicus et al., 2006; Verbeke and Molenberghs, 2003). However, this result depends on the assumption of independent and identically distributed (i.i.d.) data (Crainiceanu, 2008; Crainiceanu and Ruppert, 2004a, b, c), which is violated in the heritability problem. It has been shown that 0 values occur at a rate greater than 50%, producing conservative inferences (Blangero et al., 2013; Crainiceanu and Ruppert, 2004a; Shephard, 1993; Shephard and Harvey, 1990).

As with most statistical models, the quantitative genetic models used here are based on an assumption of multivariate Gaussianity, and this assumption is the basis of the estimation and test procedures described above. However, the heritability test statistic's null distribution may be inaccurate even when Gaussianity is perfectly satisfied, due to the limitations of the 50:50  $\chi^2$  result just mentioned. Further, for neuroimaging spatial statistics, like family-wise error (FWE) corrected inference with either voxel- or cluster-wise inference, the relevant parametric null distributions are intractable. While random field theory (Worsley et al., 1992; Friston et al., 1994; Nichols and Hayasaka, 2003) results exist for  $\chi^2$  images (Cao, 1999), they are not directly applicable here as the test statistic image cannot be expressed as a linear combination of component error fields.

Hence, there is a compelling need for alternative inference procedures that make fewer assumptions. Permutation tests are a type of nonparametric test that can provide exact control – or approximately exact when there are nuisance variables – over false positive rates. These tests depend only on minimal assumptions, namely, that under the null hypothesis the data is exchangeable, that is, that the joint distribution of the data remains unaltered after permutation (Nichols and Holmes, 2002; Winkler et al., 2014).

There is relatively little work on permutation tests for variance component inference. The typical application of variance components models is not in quantitative genetics, but in hierarchical linear models where observational units are nested in clusters, such as repeated measures designs. Of the few permutation methods proposed in this setting, they all permute the residuals (after removing the covariate effects) between and within clusters while fixing the model structure. While these procedures use different test statistics, e.g. Fitzmaurice and Lipsitz (2007) used the LRT as the statistic, while Lee and Braun (2012) used the sample variance of estimated random effect, they generally require iterative optimization of the likelihood function, and thus as permutation procedures they are yet more computationally demanding.

Samuh et al. (2012) presented a fast permutation test, though it is only applicable to the random intercept model. And recently Drikvandi et al. (2013) introduced a fast permutation test based on the variance least square estimator, which in essence fits a regression model to squared residuals. However, this approach is not based on maximum likelihood, and is only intended for a standard repeated measures model, where independent subjects are recorded multiple times, not multiple dependent subjects as in a pedigree study.

Our group presented a method to accelerate maximum likelihood estimation by applying an orthonormal data transformation that diagonalizes the phenotypic covariance, transforming a correlated heritability model into an independent but heterogeneous variance model (Blangero et al., 2013). However, this advance doesn't eliminate iterative optimization nor possible convergence problems.

In the present work, we expanded upon this work to derive approximate, non-iterative estimates and test statistics based on the first iteration of Newton's method. These procedures can be constructed with an auxiliary model based on regressing squared residuals on the kinship matrix eigenvalues. Then the Wald and score hypothesis tests can then be seen as generalized and ordinary explained sum of squares of the

auxiliary model. In addition, as the null hypothesis of no heritability corresponds to homogeneous variance of the transformed phenotype, we draw from the statistical literature on tests of heteroscedasticity for a new and completely different test for heritability detection. We develop permutation test procedures for each of these methods, thus providing FWE-corrected voxel- and cluster-wise inferences.

The remainder of this paper is organized as follows. In the next section we detail the statistical model used and describe each of our proposed methods. The simulation framework used to evaluate the methods, and the real data analysis used for illustration are described in the Evaluation section. We then present and interpret results, and offer concluding remarks.

## Theory

In this section we detail the statistical models used, introduce our fast heritability estimators and tests, and then propose several permutation strategies for these tests.

### Original and eigensimplified polygenic models

At each voxel/element, a polygenic model for the phenotype  $Y$  measured on  $N$  individuals can be written as

$$Y = X\beta + g + \epsilon \quad (1)$$

where  $X$  is an  $N \times p$  matrix consisting of an intercept and covariates, like age and sex;  $\beta$  is the  $p$ -vector of regression coefficients;  $g$  is the  $N$ -vector of latent (unobserved) additive genetic effect; and  $\epsilon$  is the  $N$ -vector of residual errors. In this study we consider the most common variance components model, with only additive and unique environmental components.

The trait covariance,  $\text{Var}(Y) = \text{Var}(g + \epsilon) = \Sigma$  can be written as

$$\Sigma = 2\sigma_A^2\Phi + \sigma_E^2I, \quad (2)$$

where  $\Phi$  is the kinship matrix;  $\sigma_A^2$  and  $\sigma_E^2$  are the additive genetic and the environmental variance components, respectively; and  $I$  is the identity matrix. The kinship matrix is comprised of kinship coefficients, half the expected proportion of genetic material shared between each pair of individuals (Lange, 2003).

The narrow sense heritability is

$$h^2 = \frac{\sigma_A^2}{\sigma_A^2 + \sigma_E^2}. \quad (3)$$

Maximum likelihood is used for parameter estimation with the assumption that the data follows a multivariate normal distribution. The log likelihood for the untransformed model (Eqs. (1) & (2)) is

$$\ell(\beta, \Sigma; Y, X) = -\frac{1}{2}N\log(2\pi) - \frac{1}{2}\log(|\Sigma|) - \frac{1}{2}(Y - X\beta)' \Sigma^{-1}(Y - X\beta). \quad (4)$$

For large datasets with arbitrary family structure, the computational burden of evaluating of the likelihood can be substantial. In particular, a quadratic form of the inverse covariance,  $\Sigma^{-1}$ , must be computed, along with the determinant of  $\Sigma$ . We take the approach of Blangero et al. (2013), who proposed an orthogonal transformation based on the eigenvectors of the kinship matrix, thus diagonalizing the covariance and simplifying the computation of the likelihood (Eq. (4)).

The eigensimplified polygenic model is obtained by transforming the data and model with a matrix  $S$ , the matrix of eigenvectors of  $\Phi$  which are the same as the eigenvectors of  $\Sigma$ , Eq. (2). Applying this transformation to Eq. (1) gives the transformed model

$$S'Y = S'X\beta + S'g + S'\epsilon$$

186 which we write as

$$Y^* = X^* \beta + \varepsilon^*, \tag{5}$$

187 where  $Y^*$  is the transformed data,  $X^*$  are the transformed covariates and  
 188  $\varepsilon^*$  is the transformed random component, where  $\varepsilon^*$  now encompasses  
 189 both the genetic and non-genetic random variations. The diagonalizing  
 190 property of the eigenvectors then gives a simplified form for the  
 variance:

$$\text{Var}(\varepsilon^*) = \Sigma^* = \sigma_A^2 D_g + \sigma_E^2 I, \tag{6}$$

192 where  $\Sigma^*$  is the variance of the transformed data and  $D_g = \text{diag}\{\lambda_{gi}\}$  is a  
 diagonal matrix of the eigenvalues of  $2\Phi$ .

193 The log likelihood takes on the exact same form as Eq. (4) for  $Y^*, X^*, \beta$   
 194 and  $\Sigma^*$ , except is much easier to work with since  $\Sigma^*$  is diagonal:

$$\ell(\beta^*, \sigma_A^2, \sigma_E^2; Y^*, X^*) = -\frac{1}{2} N \log(2\pi) - \frac{1}{2} \sum_{i=1}^N \log(\sigma_A^2 \lambda_{gi} + \sigma_E^2) - \frac{1}{2} \sum_{i=1}^N \frac{\varepsilon_i^{*2}}{\sigma_A^2 \lambda_{gi} + \sigma_E^2}.$$

196 Note that, while  $S'$  can be seen as a semi-whitening step, the trans-  
 197 formed model can also be seen as a change of variables, where the  
 198 variance is reparametrized as  $\Sigma = S \Sigma^* S'$ . As a reparametrization, the in-  
 199 variance property of maximum likelihood guarantees that the same  
 200 values of  $\beta, \sigma_A^2$  and  $\sigma_E^2$  will optimize both the original and transformed  
 201 likelihoods.

202 Use of this transformation has two major benefits. First, optimization  
 203 time is substantially reduced, as the inverse and determinant of the  
 204 transformed covariance are now trivial. Second, applying standard statisti-  
 205 cal inference procedures, including the score and the Wald test, to the  
 206 eigensimplified polygenic model produces simple algebraic forms  
 207 that can be harnessed for fast approximations. Both of these speed im-  
 208 provements facilitate the use of permutation tests that avoid asymptotic  
 209 approximations.

210 *Heritability estimation and test statistics*

211 We segregate the transformed model parameters into fixed  $\beta$  and  
 212 random  $\theta = (\sigma_A^2, \sigma_E^2)$  terms, and estimate them by maximizing the like-  
 213 lihood function via iterative numerical methods. Here, we consider  
 214 Newton's method because it leads to computationally efficient heritabil-  
 215 ity estimators and associated tests. Newton's method requires the score  
 216 and expected information matrix of the transformed model, which are

$$S(\beta, \theta) = \begin{bmatrix} X^{*'} \Sigma^{*-1} \varepsilon^* \\ -\frac{1}{2} [U' \Sigma^{*-1} \mathbf{1} - U' \Sigma^{*-2} \varepsilon^{*2}] \end{bmatrix} \tag{7}$$

218 and

$$I(\beta, \theta) = \begin{bmatrix} X^{*'} \Sigma^{*-1} X^* & 0 \\ 0 & \frac{1}{2} U' \Sigma^{*-2} U \end{bmatrix}, \tag{8}$$

219 respectively, where  $U = [\mathbf{1}, \lambda_g]$  is a  $N \times 2$  matrix,  $\mathbf{1}$  is a  $N \times 1$  vector  
 220 of ones and  $\lambda_g = \{\lambda_{gi}\}$  is a  $N \times 1$  vector of kinship matrix eigenvalues.  
 221 It is useful to write  $f^*$  for the vector with elements  $f_i^* = \hat{\varepsilon}_i^{*2}$ , where  $\hat{\varepsilon}^* =$   
 222  $Y^* - X^* \hat{\beta}$  are the transformed model residuals. Newton's method gives  
 update equations for  $\hat{\beta}$  and  $\hat{\theta}$  at iteration  $j + 1$  as:

$$\hat{\beta}_{j+1} = \left( X^{*'} (\hat{\Sigma}_j^*)^{-1} X^* \right)^{-1} X^{*'} (\hat{\Sigma}_j^*)^{-1} Y^* \tag{9}$$

$$\hat{\theta}_{j+1} = \max \left\{ 0, \left( U' (\hat{\Sigma}_j^*)^{-1} U \right)^{-1} U' (\hat{\Sigma}_j^*)^{-1} f_j^* \right\}, \tag{10}$$

227 where  $j$  indexes iteration; the variance parameters  $\theta$  must be positive,  
 228 hence the maximum operator. When these updates are iterated until  
 convergence as usual, we denote the estimates with a ML subscript, e.g.

$$\hat{\beta}_{ML}, \hat{\theta}_{ML} \text{ and } \hat{h}_{ML}^2 = \hat{\sigma}_{A,ML}^2 / (\hat{\sigma}_{A,ML}^2 + \hat{\sigma}_{E,ML}^2). \tag{229}$$

230 To allow for potential improvements on speed, we also consider a  
 231 one-step estimator. First, observe that since  $\Sigma^*$  is diagonal, Eq. (9) is  
 232 the Weighted Least Squares (WLS) regression of  $Y^*$  on  $X^*$ , and Eq. (10)  
 233 is based on the WLS regression of  $f_j^*$  on  $U$ . This immediately suggests ini-  
 234 tial values based on Ordinary Least Squares (OLS),

$$\hat{\beta}_{OLS} = \left( X^{*'} X^* \right)^{-1} X^{*'} Y^* \tag{236}$$

$$\hat{\theta}_{OLS} = \max \left\{ 0, \left( U' U \right)^{-1} U' f_{OLS}^* \right\}, \tag{11}$$

237 where  $f_{OLS}^*$  is the square of the OLS residuals

$$\hat{\varepsilon}_{OLS} = Y^* - X^* \hat{\beta}_{OLS}; \tag{12}$$

238 while not recommended as a final estimate, it also produces  $\hat{h}_{OLS}^2 =$   
 239  $\hat{\sigma}_{A,OLS}^2 / (\hat{\sigma}_{A,OLS}^2 + \hat{\sigma}_{E,OLS}^2)$ . Finally, our proposed one-step estimators are:

$$\hat{\beta}_{WLS} = \left( X^{*'} (\hat{\Sigma}_{OLS}^*)^{-1} X^* \right)^{-1} X^{*'} (\hat{\Sigma}_{OLS}^*)^{-1} Y^* \tag{242}$$

$$\hat{\theta}_{WLS} = \max \left\{ 0, \left( U' (\hat{\Sigma}_{OLS}^*)^{-1} U \right)^{-1} U' (\hat{\Sigma}_{OLS}^*)^{-1} f_{OLS}^* \right\}, \tag{13}$$

243 where  $\hat{\Sigma}_{OLS}^*$  is formed by  $\hat{\theta}_{OLS} = (\sigma_{A,OLS}^2, \sigma_{E,OLS}^2)$ , also producing  $\hat{h}_{WLS}^2 =$   
 244  $\hat{\sigma}_{A,WLS}^2 / (\hat{\sigma}_{A,WLS}^2 + \hat{\sigma}_{E,WLS}^2)$ .

245 Amemiya (1977) showed that such one-step maximum likelihood  
 246 estimators are asymptotically normal and consistent. Going forward,  
 247 we will use "ML" to refer to the maximum-likelihood, iterated estimator  
 248 and "WLS" to refer to this one-step estimator. 249

250 *Test statistics*

251 In this section we describe likelihood ratio tests (LRTs), Wald tests,  
 252 and score test for hypothesis tests of nonzero heritability; we also add  
 253 an additional test based on detecting heterogeneous variance structure  
 254 to detect heritability. We only consider the transformed model, and  
 255 tests on  $H_0: \sigma_A^2 = 0$  vs.  $H_1: \sigma_A^2 > 0$ , equivalent to inference for heritability  
 256 (Eq. (3)). Table 1 organizes the models and test statistics we consider.

257 *Likelihood ratio test*

258 The LRT (Neyman and Pearson, 1933) statistic is twice the difference  
 259 of the log-likelihoods, unrestricted minus  $H_0$ -restricted. For ML this  
 260 requires optimizing the likelihood function twice, once under the null  
 261  $H_0: \sigma_A^2 = 0$ , and once under the alternative (though the null model  
 262 is trivial, equivalent to OLS). We denote the test statistic for this test  
 263  $T_{L,ML}$ . In addition, LRT can be constructed for the transformed model in  
 264 terms of the one-step WLS estimator; we denote this statistic as  $T_{L,WLS}$ .

265 *Wald test*

266 The Wald test consists of a quadratic form of the parameter estimate  
 267 minus its null value, and its inverse asymptotic variance (i.e. expected  
 268 Fisher's information matrix). Both the estimate and its variance are  
 269 computed under the full, alternative model. 269



**Table 1**  
Comparison of model and test statistic properties. Usual P-values and CI's (confidence Intervals) refer to the best practice inference tools used with maximum likelihood estimation.

Model name	Model expression	Estimation method	Test statistics			
			LRT	WALD	Score	GQ
Original	$Y = X\beta + g + \varepsilon$	ML	(usual P-values)	(usual CI's)		
Transformed	$Y^* = X^*\beta + \varepsilon^*$	WLS, "1 Step"	$T_{L,WLS}$	$T_{W,WLS}$	$T_S$	
Transformed, split	$Y_A^* = X_A^*\beta_A + \varepsilon_A^*$ $Y_B^* = X_B^*\beta_B + \varepsilon_B^*$	ML, fully converged OLS, "0 Step"	$T_{L,ML}$	$T_{W,ML}$		$T_{GQ}$

The Wald test for the ML estimator (Rao, 2008) is

$$T_{W,ML} = \frac{1}{2} (\hat{\sigma}_{A,ML}^2)^2 [C(U' \hat{\Sigma}_{ML}^{-2} U)^{-1} C']^{-1}$$

$$= \frac{1}{2} \left( N - (\mathbf{1}' \hat{\Sigma}_{ML}^{-1} \mathbf{1})^2 (\mathbf{1}' \hat{\Sigma}_{ML}^{-2} \mathbf{1})^{-1} \right)$$

where  $C = [0 \ 1]$  is a contrast row vector, and the latter is a simpler form found in Buse (1984). Iterative optimization is required for  $T_{W,ML}$ , though it can considerably be more amenable to compute than LRT because the likelihood function is optimized only once.

The Wald test for our one-step WLS estimator can be written as

$$T_{W,WLS} = \frac{1}{2} (\hat{\sigma}_{A,WLS}^2)^2 [C(U' \hat{\Sigma}_{WLS}^{-2} U)^{-1} C']^{-1}$$

$$= \frac{1}{2} (\hat{\sigma}_{A,WLS}^2)^2 \times (\hat{\Sigma}_{OLS}^{-1} \lambda_g)' \left( I - \hat{\Sigma}_{OLS}^{-1} \mathbf{1} (\hat{\Sigma}_{OLS}^{-1} \mathbf{1})' (\hat{\Sigma}_{OLS}^{-1} \mathbf{1}) \right)^{-1} \mathbf{1}' \hat{\Sigma}_{OLS}^{-1} \lambda_g$$

where the second line shows the computation to be half the generalized explained sum of squares (Buse, 1973, 1979) of an auxiliary model, the weighted least squares regression of  $f_{OLS}^*$  on  $\lambda_g$ , with weights determined by  $\hat{\Sigma}_{OLS}^{-1}$ .

**Score test**

The score test (Rao, 2008), also known as the Lagrange multiplier test, is a quadratic form of the score (the gradient of the log likelihood) and the expected Fisher's information, each evaluated under the null hypothesis. Among the tests that we consider, the score test is the least computationally demanding procedure, as it only requires estimation of the null model. For  $H_0 : \sigma_A^2 = 0$ , the score test with the transformed likelihood function is:

$$T_S = \frac{\lambda_g' \hat{\Sigma}_{OLS}^{-2} f_{OLS}^* - \lambda_g' \hat{\Sigma}_{OLS}^{-1} \mathbf{1}}{CU' \hat{\Sigma}_{OLS}^{-2} UC'}$$

$$= \frac{1}{2} \left( \frac{\hat{\sigma}_{A,OLS}^2}{\hat{\sigma}_{OLS}^2} \right)^2 \lambda_g' \left( I - \frac{\mathbf{1}' \mathbf{1}}{N} \right) \lambda_g$$

where  $\hat{\sigma}_{OLS}^2 = (\hat{\varepsilon}_{OLS})' \hat{\varepsilon}_{OLS} / N$  is the OLS naive residual variance estimator. Similar to the Wald test,  $T_S$  can be obtained as half the regression sum of squares of an auxiliary model, the (unweighted) regression of  $f^* / \hat{\sigma}_{A,OLS}^2$  on  $\lambda_g$ . As it only involves the fitted null model, it isn't associated with a WLS or ML estimate.

We note that Wald and score tests for a null hypothesis value lying on the boundary of parameter space can take a special form (Freedman, 2007; Molenberghs and Verbeke, 2007; Morgan et al., 2007; Verbeke and Molenberghs, 2007; Silvapulle, 1992; Silvapulle and Silvapulle, 1995; Verbeke and Molenberghs, 2003). However, for our model (Eq. (1)), the standard version is appropriate if the score

function is positive at the boundary value and otherwise set to zero. As any negative score values are suppressed by our non-negative constrained estimates  $\hat{\theta}_{OLS}$  (Eq. (11)) and  $\hat{\theta}_{WLS}$  (Eq. (13)), our tests are implicitly zero when needed, and thus the appropriate Wald and score tests are as given above.

All three of the LRT, Wald, and score test procedures are asymptotically equivalent but have different small-sample performance, which we evaluate below. These tests are considered to follow asymptotically a 50 : 50 mixture of  $\chi^2$  distributions with 1 and 0 DF, where 0 a DF  $\chi^2$  is a point mass at 0 (Chernoff, 1954; Self and Liang, 1987; Stram and Lee, 1994; Dominicus et al., 2006; Verbeke and Molenberghs, 2003), although it has been shown that 0 values can occur with a higher frequency, and the standard 50:50 result will tend to produce conservative inferences (Blangero et al., 2013; Crainiceanu and Ruppert, 2004a; Shephard, 1993; Shephard and Harvey, 1990).

**Goldfeld and Quandt (GQ) test**

Instead of standard likelihood theory, an alternative approach to heritability hypothesis testing can be derived from tests of heteroscedasticity. This follows for the transformed model, since the null hypothesis of no heritability corresponds to homoscedasticity of the transformed phenotype variance ( $\text{Var}(\varepsilon^*) = \sigma^2 I$ ). Thus, rejection of the hypothesis of homoscedasticity implies a rejection of the hypothesis of zero heritability. One class of such tests requires an explicit, hypothesized form for the heterogeneous variance. Another type called "nonconstructive" does not require such explicit models; one example is the Goldfeld and Quandt (1965) (GQ) test, which we propose as a test for non-zero heritability.

The GQ test partitions observations into 2 groups, A & B, based on a variable that should explain any heterogeneous variance. The test statistic then compares the ratio of OLS residual mean squares:

$$T_{GQ} = \frac{\hat{\varepsilon}_A^* \hat{\varepsilon}_A^* / (n_A - 1)}{\hat{\varepsilon}_B^* \hat{\varepsilon}_B^* / (n_B - 1)} \tag{14}$$

where subscript A refers to the high variance group, subscript B to low variance group,  $\hat{\varepsilon}_A^*$  refers to the residuals from regressing elements of  $Y^*$  in group A on corresponding rows of  $X^*$ , and likewise for  $\hat{\varepsilon}_B^*$ , finally,  $n_A$  and  $n_B$  are the number of observations in each respective group. With Gaussian errors and under a null hypothesis of homoscedasticity,  $T_{GQ}$  follows a F-distribution with degrees of freedom  $\nu_1 = n_B - p$  and  $\nu_2 = n_A - p$ , where p is the number of columns in  $X^*$ .

For the transformed data  $Y^*$ , the kinship eigenvalues order the variance of the observations when  $\sigma_A^2 > 0$ . Thus we propose to define the two groups based on  $\lambda_{gi} > 1$  and  $\lambda_{gi} \leq 1$ , where we make use of the fact  $\sum_i \lambda_{gi} / N = \text{trace}(2\Phi) / N = 1$ .

This test is only able to detect non-zero heritability and cannot produce estimates of  $h^2$ . On the other hand, the parametric null distribution of (Eq. (14)) does not depend on the mixture approximation and large sample properties, and its implementation is straightforward. To our knowledge, this is the first proposed use of a heteroscedasticity test to create an exact (non-asymptotic), non-iterative test of heritability.

355 *Permutation test for heritability inference*

356 Permutation methods can be used to construct the null sampling  
 357 distribution which can be used to produce P-values and thresholds.  
 358 For the model with only additive genetic and environmental variance  
 359 components, the null hypothesis of no heritability implies fully inde-  
 360 pendent data. Thus, if there were no nuisance variables ( $X$ ), a permuta-  
 361 tion test could be conducted by freely permuting the data ( $Y$ ). With  
 362 covariates, we must permute suitable residuals, as detailed below.

363 To conduct inference on  $\sigma_A^2$  in the presence of the nuisance param-  
 364 eters  $\beta$  and  $\sigma_E^2$ , we draw inspiration from various methods for permuta-  
 365 tion methods for the GLM (Winkler et al., 2014). For example, there  
 366 are several different permutation schemes when testing a strict subset  
 367 of all GLM regression parameters. One approach is to permute only  
 368 the column of interest in the design matrix. This approach, due to  
 369 Draper and Stoneman (1966) could be restated as isolating the portion  
 370 of the model affected by the null hypothesis, and then only permuting  
 371 that portion. This is the motivation for our first permutation strategy  
 372 (P1), where we repeatedly fit the model, but randomly permute kinship  
 373 each time.

374 Another approach is to use the reduced, null hypothesis model to  
 375 generate residuals, permute these residuals, and use them as surrogate  
 376 null data to be re-analyzed (Freedman and Lane, 1983). For the GLM,  
 377 this is the recommended approach (Winkler et al., 2014), and corre-  
 378 sponds to an ideal test where nuisance effects are removed from the  
 379 data, leaving what should be only unstructured data (under the null)  
 380 ready to be permuted. This is the motivation for permutation scheme  
 381 (P2).

382 Finally, another approach to GLM permutation testing is to use the  
 383 full, alternative hypothesis model to generate residuals, and then use  
 384 these residuals as surrogate null data to be re-fit (ter Braak, 1992).  
 385 This approach has the merit of removing all systematic variation from  
 386 the data before permutation. This is the motivation for our third and  
 387 fourth strategies (P3 & P4).

388 *Partial model permutation (P1)*

389 We implement approach P1 by permuting just the aspect of the  
 390 model tested by the  $H_0$ . For the untransformed model this corresponds  
 391 to permuting the model's covariance term to be

$$2\sigma_A^2 P \Phi P' + \sigma_E^2 I,$$

393 where  $P$  is one of  $N!$  possible  $N \times N$  permutation matrices. For the trans-  
 formed model, the permuted covariance takes the form

$$\sigma_A^2 P D_g P' + \sigma_E^2 I.$$

395

*Null model residual permutation (P2)*

396 For P2 we generate residuals under  $H_0$ :  $\sigma_A^2 = 0$ , i.e. OLS residuals  $\hat{\epsilon}_{OLS}$   
 397 (Eq. (12)). Then we permute these residuals, and add-back nuisance  
 398 (fixed) effects to generate new  $H_0$  realizations  $\tilde{Y}^*$ :

$$\tilde{Y}^* = X^* \hat{\beta}_{OLS} + P \hat{\epsilon}_{OLS}^*, \tag{15}$$

400 where the tilde ( $\tilde{\cdot}$ ) accent denotes one of many realizations, which in  
 turn are fit with the model under consideration.

401 *Full model residual permutation (P3)*

402 For P3, we start with full model residuals, i.e. either  $\hat{\epsilon}_{ML}$  or  $\hat{\epsilon}_{WLS}$ , de-  
 403 pending on the estimator used. Then we permute these residuals, and  
 404 add-back nuisance to generate new null hypothesis realizations;  
 405 e.g., for WLS:

$$\tilde{Y}^* = X^* \hat{\beta}_{WLS} + P \hat{\epsilon}_{WLS}^*. \tag{16}$$

and analogously for ML. Again, each realization  $\tilde{Y}$  is fit to the current 407  
 model.

*Full model whitened residual permutation (P4)* 408

P4 is like P3, but we go a step further and create residuals that are 409  
 whitened before permutation. For example, for WLS: 410

$$\tilde{Y}^* = P \left( \hat{\Sigma}^{*-1/2} \hat{\epsilon}_{WLS}^* \right), \tag{17}$$

and analogously for ML. Again, each realization is fit to the current 412  
 model.

In total we have introduced five different test procedures and four 413  
 permutation strategies, summarized in Table 2. 414

*Multiple testing correction* 415

416 Whether inference is conducted voxel-wise or cluster-wise, the use  
 417 of use of an uncorrected  $\alpha = 5\%$  level leads to an excess of false posi-  
 418 tives. False discovery rate correction, controlling the expected propor-  
 419 tion of false positives among all detections, is easily applied based on  
 420 uncorrected P-values alone (Genovese et al., 2002). As uncorrected per-  
 421 mutation cluster-wise P-values require an assumption of stationarity  
 422 (though see Salimi-Khorshidi et al. (2010)), FDR is generally only ap-  
 423 plied with voxel-wise P-values. Familywise error rate (FWE) correction,  
 424 controlling the chance of one or more false positives across the whole  
 425 set (family) of tests (Nichols and Hayasaka, 2003) requires the distribu-  
 426 tion of the maximum statistic, easily computed for either voxels or clus-  
 427 ter size with permutation (Nichols and Holmes, 2002).

**Evaluation** 428

*Simulation studies* 429

430 We conduct various simulation studies to evaluate proposed  
 431 methods for heritability inference on the transformed model. The first  
 432 study considers estimator bias and variance for the different methods.  
 433 The second study measures the accuracy of parametric and permutation  
 434 inference methods. Finally, the third study evaluates FWE control in an  
 435 image-wise setting for voxel and cluster-wise inferences.

436 In all simulations, the response variable is assumed to be  $Y = X\beta + \epsilon$   
 437 where  $\epsilon$  follows  $N(0, \Sigma)$ ,  $\Sigma = h^2(2\Phi) + (1 - h^2)I$ . The design matrix  $X$   
 438 consists of an intercept, a linear trend vector  $X_1$  and a quadratic vector  
 439  $X_2$  between 1 and  $-1$ , with  $\beta = [0, 0, 10]$ . Kinship structure  $\Phi$  is  
 440 based on real pedigrees (each described below), and the simulations  
 441 considered a range of true heritabilities ( $h^2 = 0, 0.2, 0.4, 0.6, 0.8$ ).

*Simulation 1* 442

443 This simulation evaluates the bias, standard deviation and mean  
 444 squared error (MSE) of the heritability estimators (ML and WLS).  
 445 The pedigrees and sample sizes used are shown in Table 3; we used ped-  
 446 igrees from the 10th Genetics Analysis Workshop (GAW10) (Mac-Cluer

**Table 2** 42.1  
 Comparison of tests for heritability inference. 42.2

Tests	$h^2$ estimates	Distribution	Type	Optimization	Permutation	42.3
$T_{L,ML}$	✓	50:50 $\chi^2_1$ and 0	Asymptotic	ML	P1, P2, P3, P4	42.4
$T_{W,ML}$	✓	50:50 $\chi^2_1$ and 0	Asymptotic	ML	P1, P2, P3, P4	42.5
$T_{W,WLS}$	✓	50:50 $\chi^2_1$ and 0	Asymptotic	WLS	P1, P2, P3, P4	42.6
$T_S$	✓	50:50 $\chi^2_1$ and 0	Asymptotic	OLS	P1, P2, P3, P4	42.7
$T_{GQ}$	✗	$F_{n_2-p, n_1-p}$	Exact	OLS	P1, P2, P3, P4	42.8

42.9 Proposed test procedures: The score test ( $T_S$ ), the Wald test and its variants in terms of  
 42.10 WLS estimators ( $T_{W,WLS}$ ) and ML estimators ( $T_{W,ML}$ ), and the LRTs in terms of the trans-  
 42.11 formed model ( $T_{L,ML}$ ). ML optimization denotes iterative optimization until convergence;  
 42.12 WLS a 1-step of Newton's method; and OLS an estimate based on (unweighted) least  
 squares.

**Table 3**  
Datasets used in simulation 1.

Datasets	Number of pedigrees	Sample size
GAW10	2	138
GAW10	9	626
GOBS	73	858
GAW10	23	1497

et al., 1997) and from the GOBS dataset (described below). Univariate data  $Y$  was simulated as per the Gaussian model described above, and 10,000 realizations were used.

**Simulation 2**

This simulation assesses the false positive rates for each method, on the basis of both parametric and permutation methods. For this analysis we used 2 pedigrees from the GAW10 dataset with 138 subjects; the small sample size was used to ‘stress test’ the methods. Univariate data  $Y$  was simulated as per the Gaussian model described above, 10,000 realizations were used, and 500 permutations for each nonparametric procedure. On the basis of Simulations 1 and 2, ‘winner’ tests and a permutation strategy were chosen and fed into the 3rd simulation study.

**Simulation 3**

Image simulations were conducted under the null hypothesis ( $h^2 = 0$ ) on a  $96 \times 96 \times 20$  image that the response variable for each voxel are simulated as described above, smoothed with a Gaussian filter with a Full Width at Half Maximum of 4 mm. To avoid edge effects, larger images were simulated, smoothed and then truncated. For each realization we collected empirical null distributions of maximum

**Table 4**  
Simulation 2 result, comparing parametric rejection rates (percent), 5% nominal. For GAW10 data with 2 families, 138 subjects, 10,000 realizations. GQ test has the most accurate false positive rate, LRT with ML ( $T_{L,ML}$ ) is the most powerful; both GQ ( $T_{GQ}$ ) and score ( $T_S$ ) test have good power (95% MC CI for 0.05, i.e. for the null case is (4.57%, 5.42%)).

Test	True effect ( $h^2$ )				
	0	0.2	0.4	0.6	0.8
$T_S$	3.76	40.66	76.76	94.32	98.94
$T_{W,WLS}$	1.56	26.94	73.46	95.62	99.64
$T_{W,ML}$	2.50	33.00	77.74	94.84	97.54
$T_{L,ML}$	3.16	42.28	81.80	96.40	98.90
$T_{GQ}$	4.36	35.60	78.22	96.50	99.70

statistic and maximum cluster size to compute FWE P-values; we considered different cluster forming thresholds (parametric uncorrected P-value = 0.05, 0.01, 0.005, 0.001). We generated 5000 realizations and used 500 permutations with each synthetic dataset.

**Application in diffusion tensor imaging data**

We used data from the Genetics of Brain Structure and Function Study (GOBS) (Olvera et al., 2011; McKay et al., 2014) to perform voxel and cluster-wise FA heritability inference in healthy subjects. The sample comprised 859 Mexican–American individuals from 73 extended pedigrees (average size 17.2 people, range = 1–247). The sample was 59% female (351 men/508 women) and had a mean age of 43.2 (SD = 15.0; range = 19–85). All participants provided written informed consent on forms approved by the Institutional Review Boards at the University of Texas Health Science Center San Antonio (UTHSCSA) and Yale University.

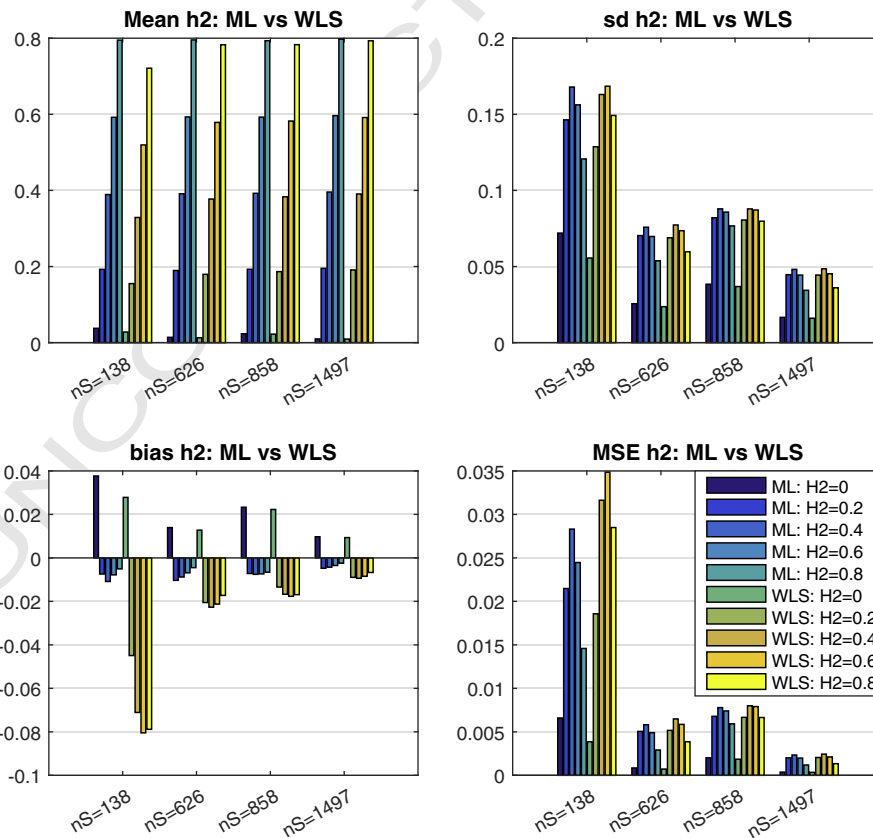


**Fig. 1.** Simulation 1 results, comparing ML and WLS behavior in terms of mean estimate (top left; true  $h^2$  varies on abscissa within clusters), standard deviation (SD; top right), bias (lower left), and mean squared error (MSE; bottom right). See Table 3 for details of each pedigree; nS denotes number of subjects. WLS has worse bias than ML, but small in absolute magnitude, leading to quite similar MSE for large samples.

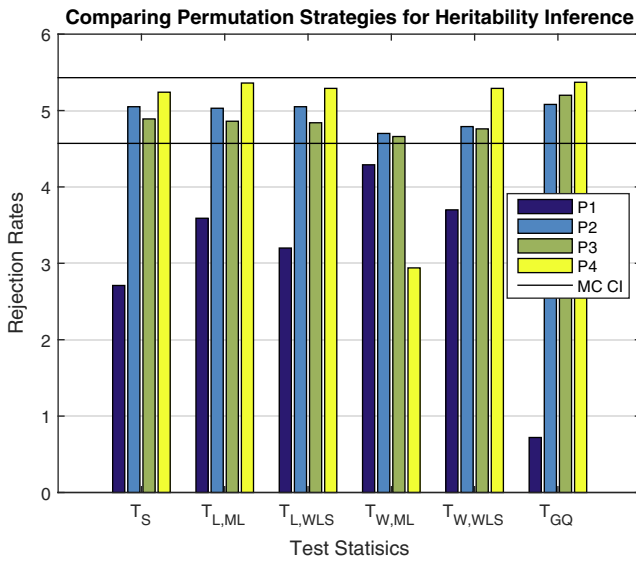


**Fig. 2.** Simulation 2 results, false positive rates for heritability permutation inference, 5% nominal. Based on GAW10 data with 2 families, 138 subjects, 10,000 realizations, and 500 permutations each realization. Monte Carlo confidence interval (MC CI) is (4.57%, 5.43%). Permutation schemes P2–P4 generally seem to work well, while  $T_{W,ML}$  tends to be conservative.

482 Diffusion imaging was performed at the Research Imaging Center,  
 483 UTHSCSA, on a Siemens 3 T Trio scanner using a multi-channel phased  
 484 array head coil. A single-shot single refocusing spin-echo, echo-planar  
 485 imaging sequence was used to acquire diffusion-weighted data with a  
 486 spatial resolution of  $1.7 \times 1.7 \times 3.0$  mm. The sequence parameters  
 487 were: TE/TR = 87/8000 ms, FOV = 200 mm, 55 isotropically distributed

diffusion weighted directions, two diffusion weighting values,  $b = 0$  488  
 and  $700 \text{ s/mm}^2$  and three  $b = 0$  (non-diffusion-weighted) images. 489

ENIGMA–DTI protocols for extraction of tract-wise average FA 490  
 values were used. These protocols are detailed elsewhere (Jahanshad 491  
 et al., 2013) and are available online [http://enigma.ini.usc.edu/](http://enigma.ini.usc.edu/protocols/dti-protocols/) 492  
[protocols/dti-protocols/](http://enigma.ini.usc.edu/protocols/dti-protocols/). Briefly, FA images from HCP subjects were 493  
 non-linearly registered to the ENIGMA–DTI target brain using FSL’s 494  
 FNIRT (Jahanshad et al., 2013). This target was created as a “minimal de- 495  
 formation target” based on images from the participating studies as pre- 496  
 viously described (Jahanshad et al., 2013b). The data were then 497  
 processed using FSL’s tract-based spatial statistics (TBSS; [http://fsl.](http://fsl.fmrib.ox.ac.uk/fsl/fslwiki/TBSS) 498  
[fmrib.ox.ac.uk/fsl/fslwiki/TBSS](http://fsl.fmrib.ox.ac.uk/fsl/fslwiki/TBSS)) analytic method (Smith et al., 2006) 499  
 modified to project individual FA values on the hand-segmented ENIG- 500  
 MA–DTI skeleton mask. The protocol, target brain, ENIGMA–DTI skele- 501  
 ton mask, source code and executables, are all publicly available 502  
 (<http://enigma.ini.usc.edu/ongoing/dti-working-group/>). The FA values 503  
 are normalized across individuals by inverse Gaussian transform 504  
 (Servin and Stephens, 2007; Allison et al., 1999) to ensure normality as- 505  
 sumption. Finally, we analyzed the voxel and cluster-wise FA values 506  
 with applying along the ENIGMA skeleton mask. To validate our pro- 507  
 posed methods for heritability estimation and inference for imaging 508  
 data, we applied them on GOBS dataset. 509

**Results** 510

*Univariate heritability simulation results* 511

*Simulation 1* 512

Fig. 1 compares WLS and ML heritability estimators for various de- 513  
 signs and effect sizes, in terms of mean, standard deviation (SD) and 514  
 mean squared error (MSE), for 10,000 Monte Carlo realizations. Large 515  
 sample theory dictates that ML should provide best performance, and 516  
 indeed it has least bias and smallest standard deviation, but the (non- 517

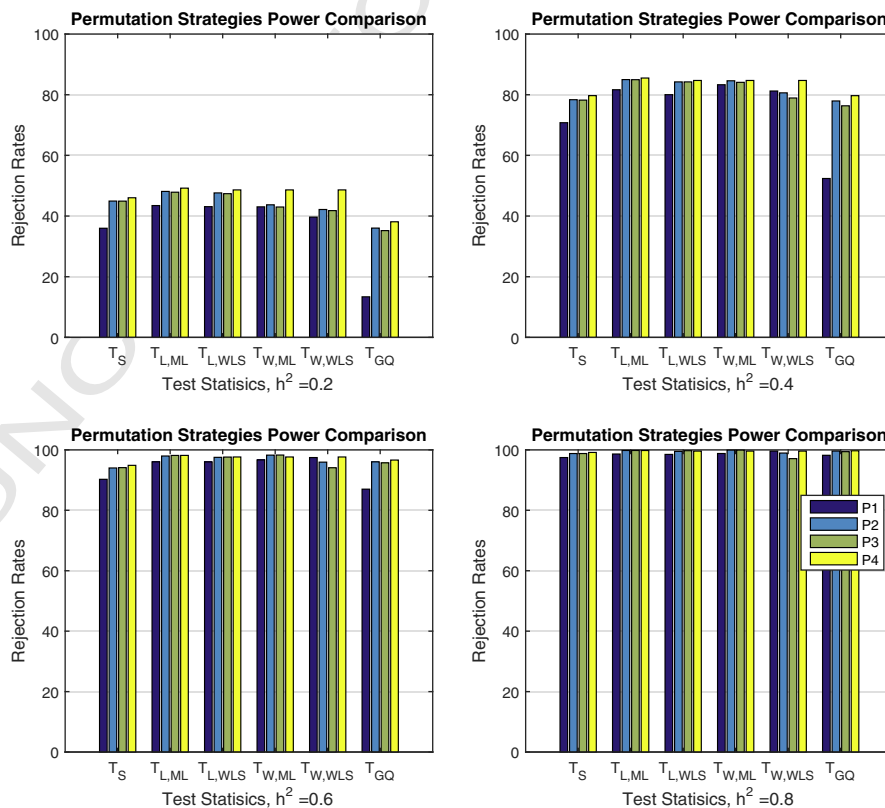


**Fig. 3.** Simulation 2 results, power for heritability permutation inference. For GAW10 data with 2 families, 138 subjects, 10,000 realizations, and 500 permutations each realization. Monte Carlo confidence interval varies with true rejection rate; for 40% it is (39.0%, 41.0%), for 80% it is (79.2%, 80.8%).



iterative) WLS has MSEs that are only slightly larger. As expected, when the sample size is increased WLS and ML heritability estimators reach almost the same performance. While the WLS estimator bias is worse (more negative) than that of ML, the absolute magnitude of bias is small in large samples.

Simulation 2

This simulation assesses the accuracy of parametric null distributions, either a 50:50  $\chi^2$  mixture or  $F$  distribution, and power. Under  $H_0$ , all false positive rates (Table 4) are conservative except  $T_{GQ}$ . The LRT and score tests have Type I error rates that are closer to the nominal level than the Wald tests for the simulated null data ( $h^2 = 0$ ) but none of them in the MC confidence interval (4.57%–5.42%). Also, the WLS Wald tests had lower error rates than ML Wald tests. In terms of power, the same pattern exists between tests and the LRT and  $T_{GQ}$  are the most powerful ones.

The conservative false positive rates are attributable to asymptotic null distributions. In particular, the 50:50 mixture approximation has recently been shown to be conservative, which we confirm here. On the other hand, parametric null distribution of  $T_{GQ}$  does not depend on a mixture approximation and, under a normality assumption, it follows  $F$ -distribution exactly; this is likely why GQ had the most accurate false positive rate (4.36%).

Figs. 2 and 3 show the performance of permutation inference, with rejection rates and power for different effect sizes under the various permutation strategies. Fig. 2 shows that, generally permutation strategy P1 is more conservative than P2, P3 and P4. Moreover the error rates in terms of P2 are close to the nominal level. Although the permutation strategy P4 has higher rejection rates, they still fall within the Monte Carlo confidence interval (4.57%–5.43%) except for  $T_{W,ML}$ .

With respect to power, Fig. 3 shows that again P2, P3 and P4 are generally superior to P1 for various effect sizes. In addition P2, P3 and P4 have almost same performance, all within the Monte Carlo confidence bounds.

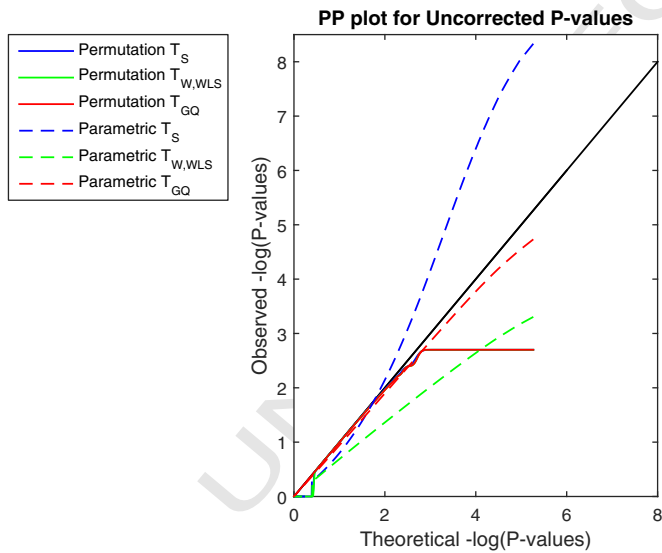


Fig. 4. Simulation 3 results,  $-\log_{10}$  PP Plot for uncorrected parametric and permutation P-values for our proposed test statistics. Permutation P-values are valid (solid lines), though are bounded below by 1/500 (above by 2.70 in  $-\log_{10}P$ ), the smallest possible permutation P-value for the 500 permutations used. The permutation P-values are overplotted here, and only the permutation  $T_{GQ}$  is visible. Parametric P-values for the non-asymptotic GQ test (dashed red line) perform well, while the parametric score test's P-values (dashed blue line) are severely anticonservative (invalid) and Wald test P-values (dashed green line) are severely conservative. Different behavior is seen for P-values larger than 0.5 (smaller than 0.70 in  $-\log_{10}P$ ) as tests giving  $\approx 50\%$  zero values produce  $\approx 50\%$  P-values of 1 (0 in  $-\log_{10}P$ ). Results based on GAW10 data with 2 families, 138 subjects, 5000 realizations, 500 permutations each realization, and  $96 \times 96 \times 20$  images with 4 mm FWHM smoothing.

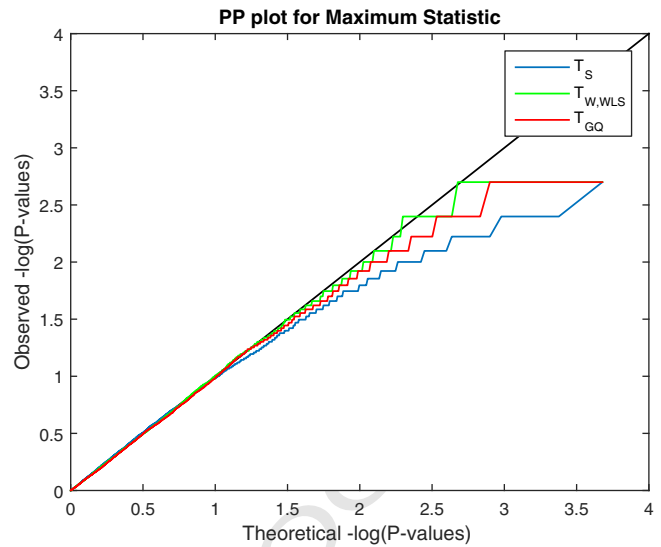


Fig. 5. Simulation 3 results,  $-\log_{10}$  PP plot for voxel-wise FWE permutation P-values under the null hypothesis, for three of our proposed test statistics. Each FWE P-value is for the maximum voxel-wise test statistic in each realized dataset. All three test statistics produce valid P-values, though are bounded below by 1/500 (above by 2.70 in  $-\log_{10}P$ ). The Wald test's FWE is slightly conservative, and score a bit more so. Results based on GAW10 data with 2 families, 138 subjects, 5000 realizations, 500 permutations each realization, and  $96 \times 96 \times 20$  images with 4 mm FWHM smoothing.

Based on all of these results, we selected  $T_S$ ,  $T_{W,WLS}$  and  $T_{GQ}$  and P2 as the computationally most efficient tests to be considered in the image-wise simulations.

Image-wise simulation results

Simulation 3

This simulation evaluates false positive rate control in the more challenging image-wise setting, for both voxel and cluster-wise heritability inference. Fig. 4 shows the P–P plot of uncorrected P-values, plotted

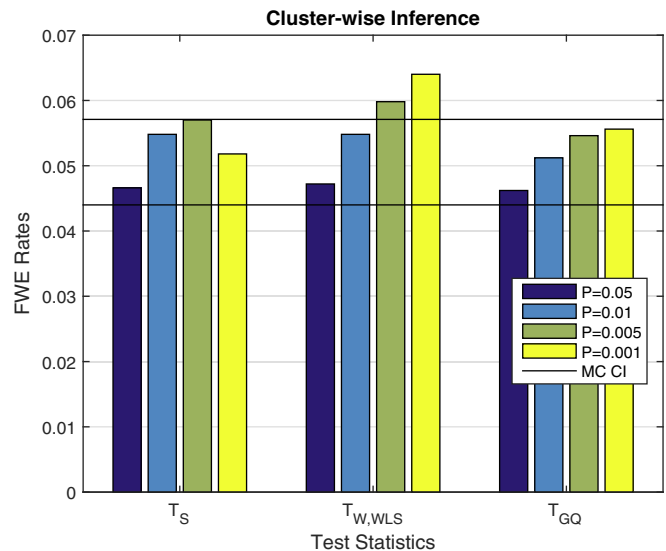
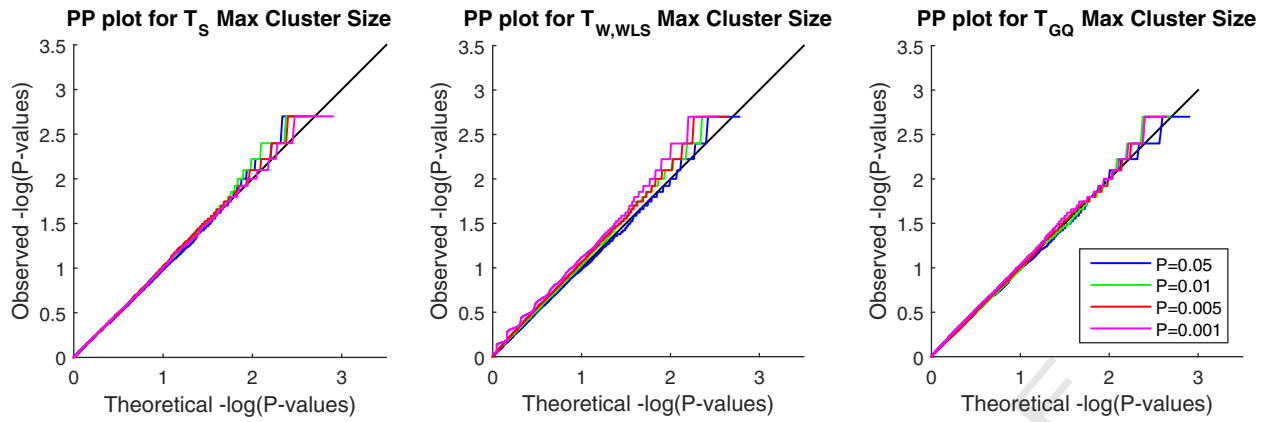


Fig. 6. Simulation 3 results, FWE error rates for cluster-wise permutation heritability inference under the null hypothesis, for three of our proposed test statistics. Score and GC test have nominal false positive rates, while the Wald test is anticonservative for high (uncorrected P of 0.005 & 0.001) clustering forming thresholds. This is likely due to use of parametric cluster-forming threshold; see text for more discussion. Results based on GAW10 data with 2 families, 138 subjects, 5000 realizations, 500 permutations each realization. Monte Carlo 95% confidence interval (4.40%, 5.60%).





**Fig. 7.** Simulation 3 results,  $-\log_{10}$  PP plots for cluster-wise FWE permutation P-values under the null hypothesis, for three of our proposed test statistics. Each FWE P-value is for the maximum cluster size in each realized dataset. GQ has most accurate FWE P-values, followed by the score test; Wald is slightly anticonservative for high cluster forming thresholds; see text for discussion. For GAW10 data with 2 families, 138 subjects, 5000 realizations, 500 permutations each realization (MC CI = (4.40, 5.60)).

559 as  $-\log_{10}P$ -values. Except for modest conservativeness ( $P \approx 10^{-2.5}$ ),  
 560 and of course the truncation due to limited permutations (500 permutations,  
 561 minimal P-value of 0.002, maximum  $-\log_{10}P$ -value of 2.69), the accuracy is quite good over-all. Fig. 5 show that FWE-corrected P-values are also accurate, with slight conservativeness with the GQ test. For the 5% level specifically, voxel-wise FWE for the score, the Wald and the GQ tests were 5.08 %, 5.44 % and 5.4 % respectively, well within the Monte Carlo 95% CI, (4.40%–5.60%).

567 Fig. 6 shows cluster-wise FWE rates for different cluster forming thresholds. All rates are nominal except for the higher cluster forming thresholds of  $T_{W,WLS}$  ( $P = 0.005$  &  $P = 0.001$ ). The cluster-forming thresholds come from the parametric null distribution, and Fig. 4 shows severe conservativeness for  $T_{W,WLS}$ 's parametric P-values. For example, that figure shows that when a  $P = 0.001$  uncorrected threshold is used for  $T_{W,WLS}$ , the actual false positive rate is less than 0.0001. This effect, combined with variation of effective false positive rate of the cluster-forming threshold over permutations, could explain this slight anticonservativeness.

577 Fig. 7 compares the selected test maximum cluster size P-values based on different cluster forming thresholds with their theoretical values; again  $T_{W,WLS}$  behavior for large cluster forming thresholds shows slightly inflated rejection rates.

581 *Real data analysis*

582 Voxel-wise FA heritability estimation and inference for the GOBS study are shown with ML and WLS estimators, creating four test statistic images:  $T_{L,ML}$ ,  $T_S$ ,  $T_{W,WLS}$ , and  $T_{GQ}$ ; permutation scheme P2 was used to compute uncorrected and FWE-corrected P-values. Fig. 8 shows histograms of  $h^2_{ML}$  (top) and  $h^2_{WLS}$  (bottom), showing generally the same distribution of heritability over the white matter skeleton. Fig. 10 shows  $h^2$  estimates on the TBSS skeleton. Fig. 9 directly compares WLS and ML heritability estimates with a scatter plot, showing a slight but consistent trend towards underestimation of  $h^2_{ML}$  relative to  $h^2_{WLS}$ , consistent with simulation (Fig. 1).

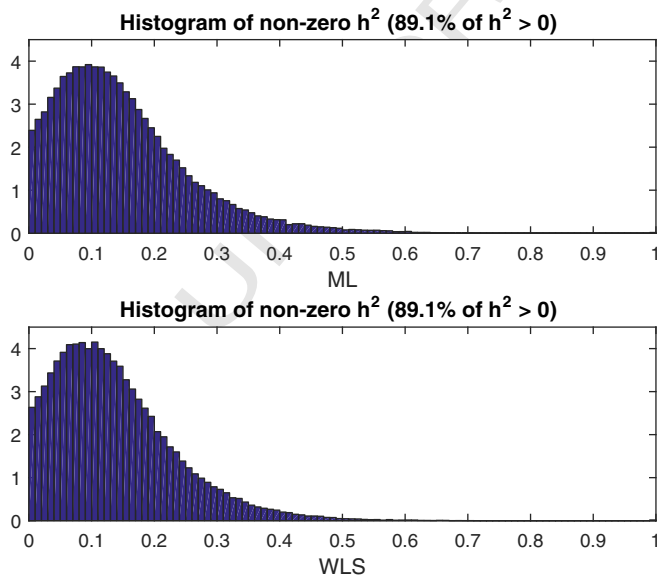


**Fig. 8.** Real data results, comparison of voxel-wise heritability estimates from ML and WLS estimates. The histograms show that the estimates from the two methods are largely similar.

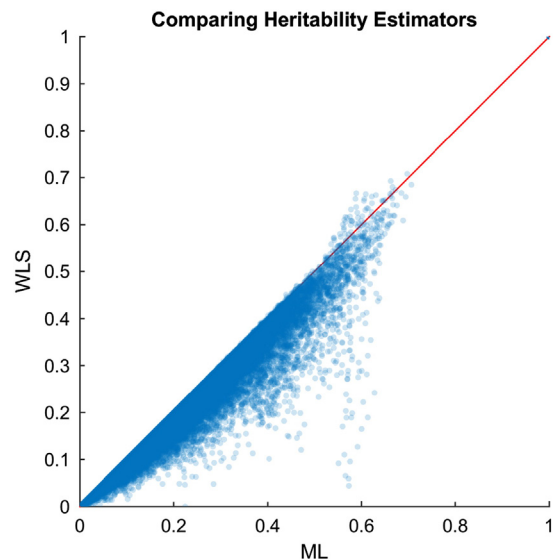


**Fig. 9.** Real data results, scatterplot of voxel-wise heritability estimates from ML and WLS estimates. The two methods are largely similar, though ML is almost always larger than WLS estimates.

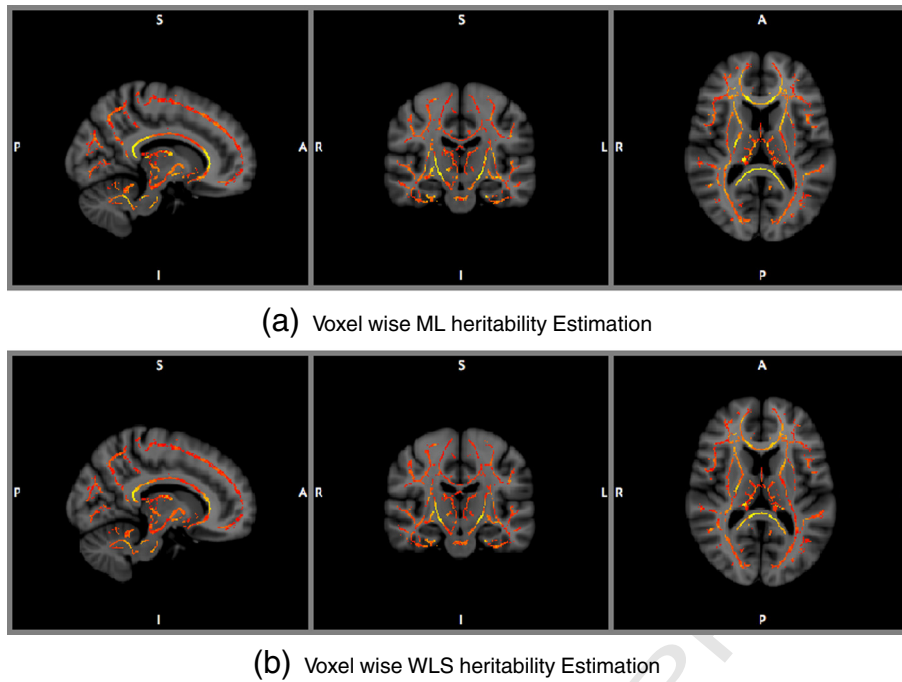


**Fig. 10.** Real data results, voxel-wise heritability estimates for ML (top) and WLS (bottom). Heritability shown in hot-metal color scale, intensity range [0, 0.5] for both, overlaid on MNI reference brain. Differences only apparent in highest FA areas.

592 Voxel-wise uncorrected  $-\log_{10}$  P-values from  $T_S$ ,  $T_{W,WLS}$ ,  $T_{GQ}$  and  
 593  $T_{L,ML}$  based on P2 are compared in Fig. 11. Considering  $T_{L,ML}$  as a refer-  
 594 ence (on the abscissa),  $T_{W,WLS}$  and  $T_{GQ}$  are generally less sensitive than  
 595  $T_{L,ML}$  (Fig. 11 middle and right panels), consistent with the simulations above.  
 596 However,  $T_S$  was more comparable with  $T_{L,ML}$  (Fig. 11 left  
 597 panel). Level 5% FWE-corrected statistic thresholds for  $T_S$ ,  $T_{W,WLS}$ ,  $T_{L,ML}$   
 598 and  $T_{GQ}$  are 39.92, 18.31, 24.27 and 1.72, respectively, producing signifi-  
 599 cant voxel counts of 8521, 1043, 7418 and 2446, respectively, out of  
 600 117,139 voxels.

601 Cluster-wise inference results for cluster forming thresholds  
 602 corresponded to uncorrected P-value = 0.01 % are shown in Table 5  
 603 the tests that we consider. Level 5% FWE-corrected cluster size thresh-  
 604 olds for  $T_S$ ,  $T_{W,WLS}$ ,  $T_{L,ML}$  and  $T_{GQ}$  are 265, 98, 142 and 135 voxels, respec-  
 605 tively. For voxel-wise inference, Fig. 12, the score test was most similar  
 606 to ML's LRT, and likewise for cluster-wise inference, Fig. 13.

## Discussion & conclusions

607

We have proposed a number of computationally efficient tests for  
 heritability with family data. To our knowledge this is the first work  
 that enables practitioners to study brain phenotype heritability in each  
 voxel without confronting an intense computational burden. Our  
 methods are based on the eigensimplified model of Blangero et al.  
 (2013), most of which can be implemented with auxiliary models, cor-  
 responding to regressing squared OLS residuals on the kinship matrix  
 eigenvalues.

615 For heritability estimation our WLS method, based on one step of  
 616 Newton's method, was a fast and reasonable approximation to fully iter-  
 617 ated ML, ideal for application to brain image data.

618 For heritability inference, we found that parametric P-values for LRT,  
 619 Wald and score methods were all conservative, likely due to the  
 620

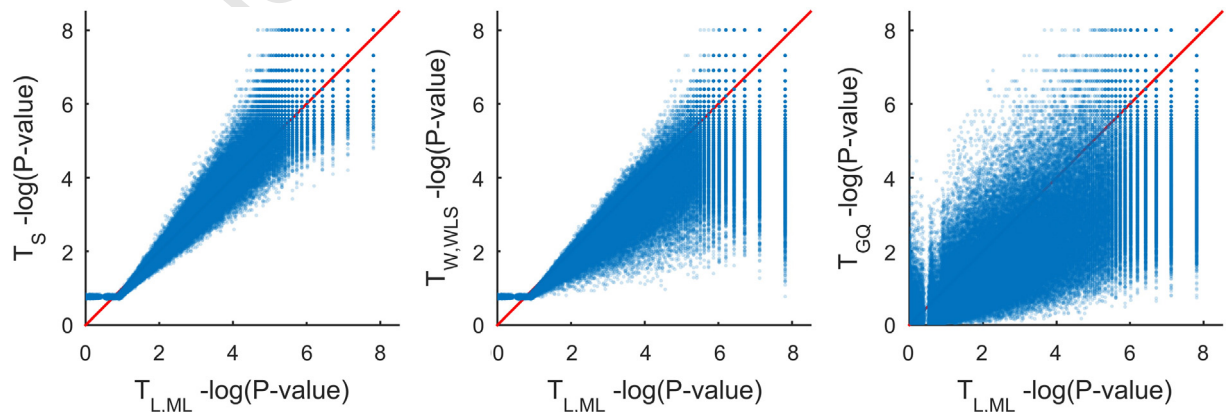


**Fig. 11.** Real data results, scatter plots of voxel-wise uncorrected  $-\log_{10}$  P-values for score, WLS Wald and GQ tests vs. the ML LRT test. Score P-values are most faithful representation of the ML LRT P-values, while WLS Wald P-values tend to be more conservative; GQ P-values are much more different and generally more conservative.

t5.1 **Table 5**  
t5.2 Real data results, cluster-wise inferences with different methods.

t5.3	Method	Total # of clusters	# of significant clusters	Largest cluster size	Smallest corrected P-value
t5.4	$T_{L,ML}$	1770	22	24,246	0.0005
t5.5	$T_{W,WLS}$	1725	19	3643	0.0003
t5.6	$T_S$	1689	11	31,250	0.0003
t5.7	$T_{GQ}$	1751	20	4383	0.0003

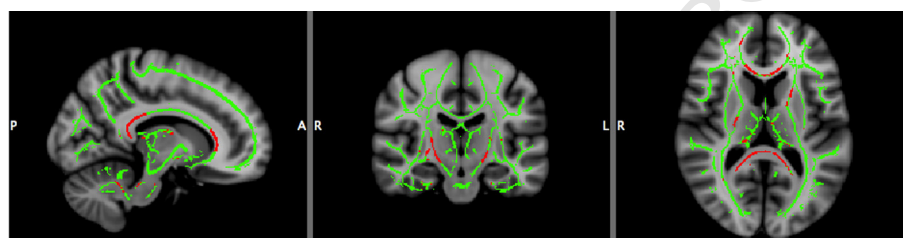
t5.8 Cluster-wise inference for  $T_{L,ML}$ ,  $T_{W,WLS}$ ,  $T_S$  and  $T_{GQ}$ . Based on 858 subjects from GOBS and  
t5.9 3000 permutations.

621 untenable i.i.d. assumption underlying the 50:50  $\chi^2$  mixture approxi-  
622 mation. As an alternative, permutation test error rates were much closer  
623 than parametric one to the nominal level. Notably, all of our simulations  
624 included fixed effects covariates ( $X$ ).

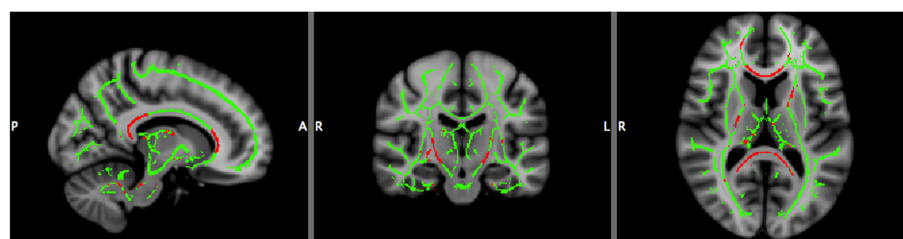
625 The GQ heteroscedasticity test, adapted here for heritability detec-  
626 tion, had good performance in simulation, with the best false positive  
627 control and respectable power, but on the real data was dramatically  
628 different (see Fig. 12) and apparently less powerful.

Image wise simulation results showed that FWE-corrected voxel- 629  
and cluster-wise inference was valid at the 5% level for  $T_S$  and  $T_{GQ}$ , per- 630  
mutation scheme P2. In real data, the P-values for  $T_{GQ}$  were less similar 631  
to the LRT results than the score or Wald test, and was less sensitive over 632  
all. The GQ test's power depends on the cut point used to define the two 633  
groups, though we did not investigate further. On balance we suggest 634  
the use of  $T_S$  for standard neuroimaging inference tool including voxel 635  
and cluster-wise inference. 636

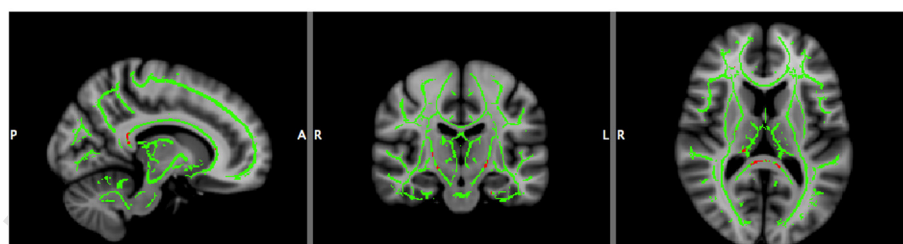
Running time for different test statistics that were presented in 637  
Table 6 based on a benchmark with Intel(R) core(TM) i7-2600 CPU @ 638  
3.4 GH and 16 GB RAM feature confirms that the empirical null distribu- 639  
tion of explained sum of squares of auxiliary model ( $T_S$ ) under the per- 640  
mutation scheme P2 can be derived substantially faster than  $T_{L,ML}$ , the 641  
classic test statistic for heritability inference. Although the sample size 642  
plays an important role in running time, we believe that  $T_S$  can be derived 643  
significantly faster than the other tests, since it does not depend on num- 644  
erical optimization. Hence, the whole permutation distribution can be 645  
derived easily, either for a univariate trait or a multivariate spatially de- 646  
pendent neuroimaging data accounting explicitly for family wise error. 647



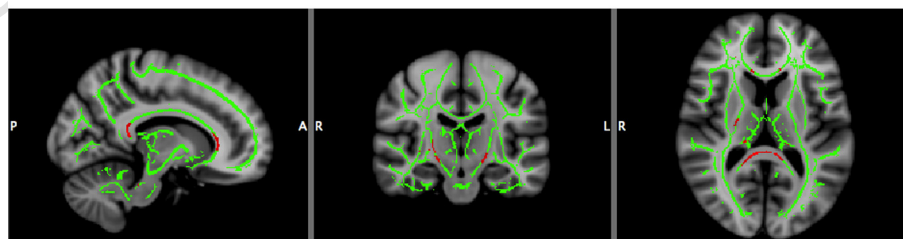
(a) LRT for ML estimator ( $T_{L,ML}$ )



(b) Score Test ( $T_S$ )



(c) WALD test for WLS estimator ( $T_{W,WLS}$ )



(d) GQ Test ( $T_{GQ}$ )

**Fig. 12.** Real data results, voxel-wise 5% FWE significant heritability, for 4 different methods. Full skeleton and significant voxels are in green and red, respectively. The non-iterative score test gives very similar results to the ML (fully iterated) LRT, with the other 2 methods being less sensitive.

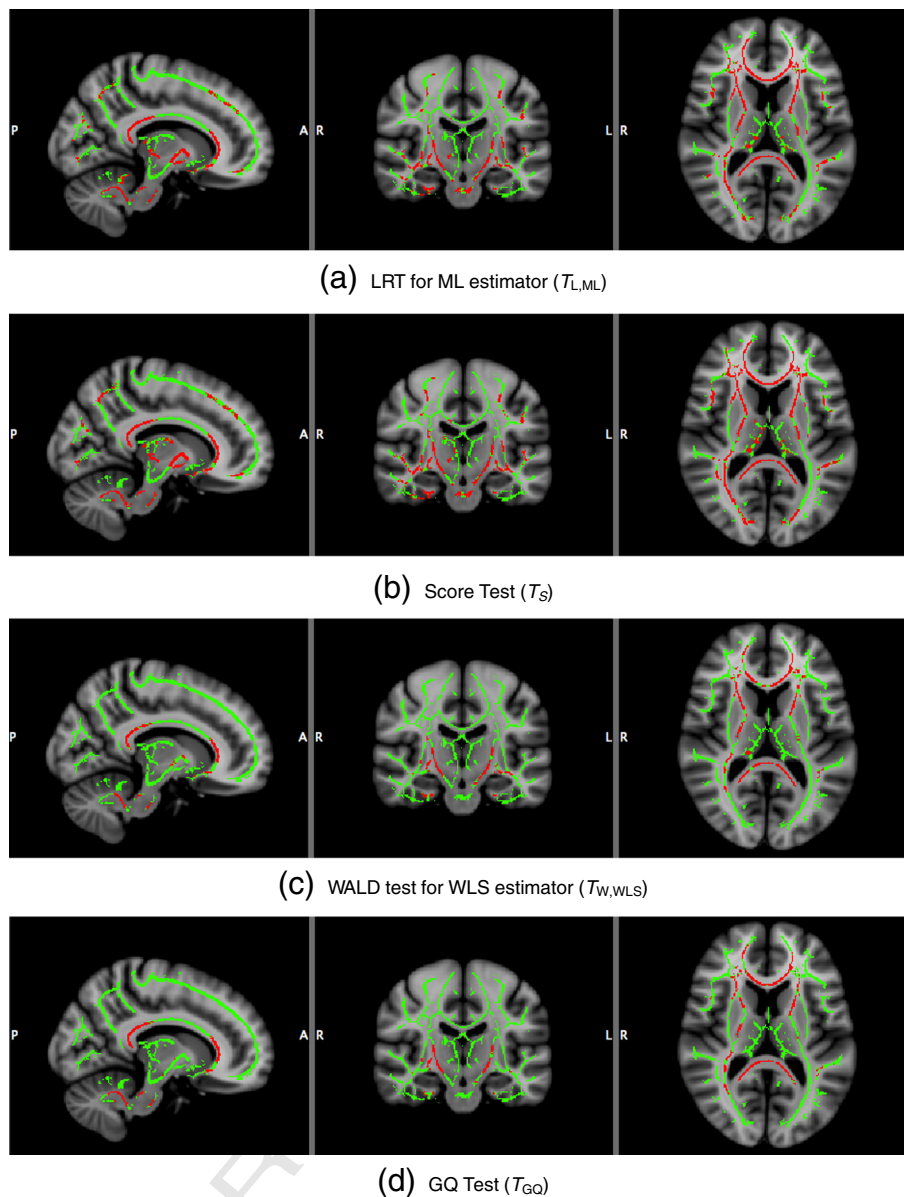


**Fig. 13.** Real data results, cluster-wise 5% FWE significant heritability, for 4 different methods, cluster-forming threshold parametric uncorrected  $P = 0.01$ . Full skeleton and significant voxels are in green and red, respectively. Methods appear more similar, but again the non-iterative score test is most similar to the ML LRT result.

648 Finally, we note that yet-more computationally efficient estimates  
 649 can be obtained by conditioning on the over-all variance estimate,  $\hat{\sigma}^2$ ,  
 650 which leads to a 1-parameter variance model. However, in initial simu-  
 651 lations we found that this lead to greater bias in  $h^2$  and specifically  $h^2$  es-  
 652 timates in excess of 1.0. Thus we retained the 2-parameter variance  
 653 model.

**Table 6**

654 Computation times. Comparison of running times for a dataset with 138 subjects, 2 fami-  
 655 lies, (GAW10 kinship) and 184,320 voxels. Run on Intel(R) core(TM) i7-2600 CPU @ 3.4  
 656 GH and 16 GB RAM.

Statistics	Univariate trait	Image-wise trait
$T_{L,ML}$	1 s	8 h
$T_{W,WLS}$	0.005 s	2 s
$T_S$	0.005 s	2 s
$T_{GQ}$	0.004 s	1.5 s

In conclusion, our results present a novel inference technique to be  
 implemented in the genetic imaging analysis software like SOLAR-  
 Eclipse ([http://www.nitrc.org/projects/se\\_linux](http://www.nitrc.org/projects/se_linux)). These methods pro-  
 vide fast inference procedure on millions of phenotypes, filtering a  
 small number of elements for further investigation with more computa-  
 tional intense tools. In future work we will extend these tools for infer-  
 ence on covariates, in particular permutation-based tests for voxel-wise  
 GWAS analysis for family based data.

#### Uncited references

Kochunov et al., In Review  
 Servin and Stephens, 07 2007

#### Acknowledgments

This study was supported by R01 EB015611 (PK, TN), MH0708143  
 and MH083824 grants to DCG and by MH078111 and MH59490 to JB.



668 This work was also supported in part by a Consortium grant  
669 (U54 EB020403) from the NIH Institutes contributing to the Big Data  
670 to Knowledge (BD2K) Initiative, including the NIBIB and NCI. TN is sup-  
671 ported by the Wellcome Trust.

## 672 References

673 Allison, D.B., Neale, M.C., Zannoli, R., Schork, N.J., Amos, C.I., Blangero, J., 1999. Testing the  
674 robustness of the likelihood-ratio test in a variance-component quantitative-trait  
675 loci-mapping procedure. *Am. J. Hum. Genet.* 650 (2), 0 531–0 544.  
676 Almasy, L., Blangero, J., 1998. Multipoint quantitative-trait linkage analysis in general  
677 pedigrees. *Am. J. Hum. Genet.* 620 (5), 0 1198–0 1211.  
678 Amemiya, T., 1977. A note on a heteroscedastic model. *J. Econ.* 60 (3), 0 365–0 370.  
679 Amos, C.I., 1994. Robust variance-components approach for assessing genetic linkage in  
680 pedigrees. *Am. J. Hum. Genet.* (3), 0 535–0 543.  
681 Blangero, J., Almasy, L., 1997. Multipoint oligogenic linkage analysis of quantitative traits.  
682 *Genet. Epidemiol.* 140 (6), 0 959–0 964.  
683 Blangero, J., Diego, V.P., Dyer, T.D., Almeida, M., Peralta, J., Kent, J.W., Williams, J.T., Almasy,  
684 L., Göring, H.H.H., 2013. A Kernel of Truth: in Variance-Component Models for Complex Human Pedigrees. vol. 81. Academic Press.  
685 Blokland, G.A., McMahon, K.L., Hoffman, J., Zhu, G., Meredith, M., Martin, N.G., Thompson,  
686 P.M., de Zubicaray, G.L., Wright, M.J., 2008. Quantifying the heritability of task-related  
687 brain activation and performance during the n-back working memory task: a twin  
688 fMRI study. *Biol. Psychol.* 790 (1), 0 70–0 79.  
689 Brouwer, R.M., Mandl, R.C., Peper, J.S., van Baal, G.C.M., Kahn, R.S., Boomsma, D.I., Pol,  
690 H.E.H., 2010. Heritability of (DTI) and (MTR) in nine-year-old children. *NeuroImage*  
691 530 (3), 0 1085–0 1092.  
692 Buse, A., 1973. Goodness of fit in generalized least squares estimation. *Am. Stat.* (3),  
693 106–108.  
694 Buse, A., 1979. Goodness-of-fit in the seemingly unrelated regressions model: a general-  
695 ization. *J. Econ.* 10.  
696 Buse, A., 1984. Tests for additive heteroskedasticity: Goldfeld and Quandt revisited. *Empir.*  
697 *Econ.* 90 (4), 0 199–0 216.  
698 Cao, J., 1999. The size of the connected components of excursion sets of  $X^2$ ,  $t$  and  $F$  fields.  
699 *Adv. Appl. Probab.* 310 (3), 0 579–0 595.  
700 Chernoff, H., 1954. On the distribution of the likelihood ratio. *Ann. Math. Stat.* 250 (3),  
701 573–578 (0 pp.).  
702 Chiang, M.-C., Barysheva, M., Shattuck, D.W., Lee, A.D., Madsen, S.K., Avedissian, C.,  
703 Klunder, A.D., Toga, A.W., McMahon, K.L., de Zubicaray, G.L., Wright, M.J., Srivastava,  
704 A., Balow, N., Thompson, P.M., 2009. Genetics of brain fiber architecture and intellec-  
705 tual performance. *J. Neurosci.* 290 (7), 0 2212–0 2224.  
706 Chiang, M.-C., McMahon, K.L., de Zubicaray, G.L., Martin, N.G., Hickie, I., Toga, A.W., Wright,  
707 M.J., Thompson, P.M., 2011. Genetics of white matter development: a (DTI) study of  
708 705 twins and their siblings aged 12 to 29. *NeuroImage (ISSN: 1053-8119)* 540 (3),  
709 0 2308–0 2317.  
710 Crainiceanu, C., 2008. Likelihood ratio testing for zero variance components in linear  
711 mixed models. In: Dunson, D. (Ed.), *Random Effect and Latent Variable Model Selection*.  
712 *Lecture Notes in Statistics* volume 192. Springer, New York, pp. 3–17.  
713 Crainiceanu, C.M., Ruppert, D., 2004 aa. Restricted likelihood ratio tests in nonparametric  
714 longitudinal models. *Stat. Sin.* 140 (3), 0 713–0 730.  
715 Crainiceanu, C.M., Ruppert, D., 2004 bb. Likelihood ratio tests in linear mixed models with  
716 one variance component. *J. R. Stat. Soc. Ser. B (Stat Methodol.)* 660 (1), 0 165–0 185.  
717 Crainiceanu, C.M., Ruppert, D., 2004 cc. Likelihood ratio tests for goodness-of-fit of a non-  
718 linear regression model. *J. Multivar. Anal.* 910 (1), 0 35–0 52.  
719 den Braber, A., Bohlken, M.M., Brouwer, R.M., Ent, D. van 't, Kanai, R., Kahn, R.S., de Geus,  
720 E.J.C., Hulshoff Pol, H.E., Boomsma, D.I., 2013. Heritability of subcortical brain mea-  
721 sures: a perspective for future genome-wide association studies. *NeuroImage* 83C,  
722 0 98–0 102.  
723 Dominicus, A., Skrondal, A., Gjessing, H., Pedersen, N., Palmgren, J., 2006. Likelihood ratio  
724 tests in behavioral genetics: problems and solutions. *Behav. Genet. (ISSN: 0001-*  
725 *8244)* 360 (2), 0 331–0 340.  
726 Draper, N., Stoneman, D., 1966. Testing for the inclusion of variables in linear regression  
727 by a randomisation technique. *Technometrics* 80 (4), 0 695–0 699.  
728 Drikvandi, R., Verbeke, G., Khodadadi, A., Partovi Nia, V., 2013. Testing multiple variance  
729 components in linear mixed-effects models. *Biostatistics* 140 (1), 0 144–0 159  
730 (Oxford, England).  
731 Fitzmaurice, G.M., Lipsitz, S.R., Ibrahim, J.G., Sept. 2007. A note on permutation tests for  
732 variance components in multilevel generalized linear mixed models. *Biometrics*  
733 630 (3), 0 942–0 946.  
734 Freedman, D., Lane, D., 1983. A nonstochastic interpretation of reported significance  
735 levels. *J. Bus. Econ. Stat.* 10 (4), 0 292–0 298.  
736 Freedman, D.a., Nov. 2007. How can the score test be inconsistent? *Am. Stat.* 610 (4), 0  
737 291–0 295.  
738 Friston, K.J., Worsley, K.J., Frackowiak, R.S.J., Mazziotta, J.C., Evans, A.C., 1994. Assessing the  
739 significance of focal activations using their spatial extent. *Hum. Brain Mapp.* 10 (3), 0  
740 210–0 220.  
741 Genovese, C.R., Lazar, N.A., Nichols, T.E., 2002. Thresholding of statistical maps in func-  
742 tional neuroimaging using the false discovery rate. *NeuroImage* 150, 0 870–0 878.  
743 Glahn, D.C., Thompson, P.M., Blangero, J., 2007. Neuroimaging endophenotypes: strategies  
744 for finding genes influencing brain structure and function. *Hum. Brain Mapp.* 280 (6),  
745 0 488–0 501.  
746 Goldfeld, S., Quandt, R., 1965. Some tests for homoscedasticity. *J. Am. Stat.* 600 (310), 0  
747 539–0 547.

Hopper, J.L., Mathews, J.D., 1982. Extensions to multi-variate normal models for pedigree  
749 analysis. *Ann. Hum. Genet.* 46, 0 373–0 383.  
750 Jahanshad, N., Kochunov, P.V., Sprooten, E., Mandl, R.C., Nichols, T.E., Almasy, L., Blangero,  
751 J., Brouwer, R.M., Curran, J.E., de Zubicaray, G.L., Duggirala, R., Fox, P.T., Hong, L.E.,  
752 Landman, B.A., Martin, N.G., McMahon, K.L., Medland, S.E., Mitchell, B.D., Olvera,  
753 R.L., Peterson, C.P., Starr, J.M., Sussmann, J.E., Toga, A.W., Wardlaw, J.M., Wright,  
754 M.J., Pol, H.E.H., Bastin, M.E., McIntosh, A.M., Deary, I.J., Thompson, P.M., Glahn, D.C.,  
755 2013. Multi-site genetic analysis of diffusion images and voxelwise heritability  
756 analysis: a pilot project of the ENIGMA-DTI working group. *NeuroImage* 810, 0  
757 455–0 469.  
758 Kochunov, P., Glahn, D., Lancaster, J., Winkler, A., Smith, S., Thompson, P., Almasy, L.,  
759 Duggirala, R., Fox, P., Blangero, J., 2010. Genetics of microstructure of cerebral white  
760 matter using diffusion tensor imaging. *NeuroImage* 530 (3), 0 1109–0 1116.  
761 Kochunov, P., Glahn, D., Lancaster, J., Thompson, P., Kochunov, V., Rogers, B., Fox, P.,  
762 Blangero, J., Williamson, D., 2011a. Fractional anisotropy of cerebral white matter  
763 and thickness of cortical gray matter across the lifespan. *NeuroImage* 580 (1), 0  
764 41–0 49.  
765 Kochunov, P., Glahn, D., Nichols, T., Winkler, A., Hong, E., Holcomb, H., Stein, J., Thompson,  
766 P., Curran, J., Carless, M., Olvera, R., Johnson, M., Cole, S., Kochunov, V., Kent, J.,  
767 Blangero, J., 2011b. Genetic analysis of cortical thickness and fractional anisotropy  
768 of water diffusion in the brain. *Front. Neurosci.* 50 (120).  
769 Kochunov, P., Jahanshad, N., Sprooten, E., Nichols, T.E., Mandl, R.C., Almasy, L., Booth, T.,  
770 Brouwer, R.M., Curran, J.E., de Zubicaray, G.L., Dimitrova, R., Duggirala, R., Fox, P.T.,  
771 Hong, L.E., Landman, B.A., Lemaître, H., Lopez, L.M., Martin, N.G., McMahon, K.L.,  
772 Mitchell, B.D., Olvera, R.L., Peterson, C.P., Starr, J.M., Sussmann, J.E., Toga, A.W.,  
773 Wardlaw, J.M., Wright, M.J., Wright, S.N., Bastin, M.E., McIntosh, A.M., Boomsma,  
774 D.I., Kahn, R.S., den Braber, A., de Geus, E.J., Deary, I.J., Pol, H.E.H., Williamson, D.E.,  
775 Blangero, J., Ent, D. van 't, Thompson, P.M., Glahn, D.C., 2014. Multi-site study of addi-  
776 tive genetic effects on fractional anisotropy of cerebral white matter: comparing  
777 meta and megaanalytical approaches for data pooling. *NeuroImage* 950, 0 136–0 150.  
778 Kochunov, P., Jahanshad, N., Marcus, D., Winkler, A., Sprooten, E., Nichols, T., Hong, L.,  
779 Behrens, T., Andersson, E., J. and Yacoub, Ugurbil, K., Brouwer, C., Landman, B.,  
780 Braber, A., Almasy, L., Fox, P., Olvera, R., Blangero, J., DC, G., Van Essen, D., 2014  
781 aw. Heritability of fractional anisotropy in human white matter: a comparison of  
782 Human Connectome Project and ENIGMA-DTI data. *NeuroImage (In Review)*.  
783 Koten, J.W., Wood, G., Hagoort, P., Goebel, R., Propping, P., Willmes, K., Boomsma, D.I.,  
784 2009. Genetic contribution to variation in cognitive function: an fMRI study in  
785 twins. *Science* 3230 (5922), 0 1737–0 1740.  
786 Kremen, W.S., Prom-Wormley, E., Panizzon, M.S., Eysler, L.T., Fischl, B., Neale, M.C., Franz,  
787 C.E., Lyons, M.J., Pacheco, J., Perry, M.E., Stevens, A., Schmitt, J.E., Grant, M.D.,  
788 Seidman, L.J., Thermenos, H.W., Tsuang, M.T., Eisen, S.A., Dale, A.M., Fennema-  
789 Notestine, C., 2010. Genetic and environmental influences on the size of specific  
790 brain regions in midlife the VETSA MRI study. *NeuroImage* 490 (2), 0 1213–0 1223.  
791 Lange, K., 2003. *Mathematical and Statistical Methods for Genetic Analysis*. 2nd ed.  
792 Springer.  
793 Lee, O.E., Braun, T.M., 2012. Permutation tests for random effects in linear mixed models.  
794 *Biometrics* 680 (2), 0 486–0 493.  
795 MacCluer, J.W., Blangero, J., Dyer, T.D., Speer, M.C., Jan. 1997. GAW10: simulated family  
796 data for a common oligogenic disease with quantitative risk factors. *Genet.*  
797 *Epidemiol.* 140 (6), 0 737–0 742.  
798 Matthews, S.C., Simmons, A.N., Strigo, I., Jang, K., Stein, M.B., Paulus, M.P., 2007. Heritabil-  
799 ity of anterior cingulate response to conflict: an fMRI study in female twins.  
800 *NeuroImage* 380 (1), 0 223–0 227.  
801 McKay, D., Knowles, E., Winkler, A., Sprooten, E., Kochunov, P., Olvera, R., Curran, J., Kent,  
802 J., Jack, W., Carless, M., GÅrning, H., Dyer, T., Duggirala, R., Almasy, L., Fox, P., Blangero,  
803 J., Glahn, D., 2014. Influence of age, sex and genetic factors on the human brain. 80  
804 (2), 0 143–0 152.  
805 Molenberghs, G., Verbeke, G., Feb. 2007. Likelihood ratio, score, and Wald tests in a  
806 constrained parameter space. *Am. Stat.* 610 (1), 0 22–0 27.  
807 Morgan, B.J.T., Palmer, K.J., Ridout, M.S., Nov. 2007. Negative score test statistic. *Am. Stat.*  
808 610 (4), 0 285–0 288.  
809 Neyman, J., Pearson, E.S., 1933. On the problem of the most efficient tests of statistical hypo-  
810 theses. *Philosophical Transactions of the Royal Society of London Series A, Contain-*  
811 *ing Papers of a Mathematical or Physical Character* 231 pp. 289–337 (0 pp).  
812 Nichols, T.E., Hayasaka, S., 2003. Controlling the familywise error rate in functional neuro-  
813 imaging: a comparative review. *Stat. Methods Med. Res.* 120 (5), 0 419–0 446.  
814 Nichols, T.E., Holmes, A.P., 2002. Nonparametric permutation tests for functional neuro-  
815 imaging: a primer with examples. *Hum. Brain Mapp.* 150 (1), 0 1–0 25.  
816 Olvera, R., Bearden, C., Velligan, D., Almasy, L., Carless, M., Curran, J., Williamson, D.,  
817 Duggirala, R., Blangero, J., Glahn, D., 2011. Common genetic influences on depression,  
818 alcohol, and substance use disorders in Mexican-American families. *Am. J. Med.*  
819 *Genet. B Neuropsychiatr. Genet.* 1560 (5), 561–568.  
820 Polk, T.A., Park, J., Smith, M.R., Park, D.C., 2007. Nature versus nurture in ventral visual cor-  
821 tex: a functional magnetic resonance imaging study of twins. *J. Neurosci.* 270 (51),  
822 13921–13925.  
823 Rao, C.R., 2008. John Wiley & Sons, Inc.  
824 Rimol, L.M., Panizzon, M.S., Fennema-Notestine, C., Eysler, L.T., Fischl, B., Franz, C.E., Hagler,  
825 D.J., Lyons, M.J., Neale, M.C., Pacheco, J., Perry, M.E., Schmitt, J.E., Grant, M.D., Seidman,  
826 L.J., Thermenos, H.W., Tsuang, M.T., Eisen, S.A., Kremen, W.S., Dale, A.M., 2010. Cortical  
827 thickness is influenced by regionally specific genetic factors. *Biol. Psychiatry* 670 (5),  
828 0 493–0 499.  
829 Salimi-Khorshidi, G., Smith, S.M., Nichols, T.E., 2010. Adjusting the effect of nonstationarity  
830 in cluster-based and TFCE inference. *NeuroImage* 540 (3), 2006–2019.  
831 Samuh, M.H., Grilli, I., Rampichini, C., Salmaso, L., Lunardon, N., 2012. The use of permu-  
832 tation tests for variance components in linear mixed models. *Commun. Stat. - Theory*  
833 *and Methods* 410 (16–17), 3020–3029.  
834

- 835 Self, S.G., Liang, K.-Y., 1987. Asymptotic properties of maximum likelihood estimators and  
836 likelihood ratio tests under nonstandard conditions. *J. Am. Stat. Assoc.* 820 (398),  
837 605–610 0 pp.
- 838 Servin, B., Stephens, M., 07 2007. Imputation-based analysis of association studies:  
839 candidate regions and quantitative traits. 30 (7).
- 840 Shephard, N., 1993. Maximum likelihood estimation of regression models with stochastic  
841 trend components. *J. Am. Stat. Assoc.* 880 (422), 590–595 (0 pp.).
- 842 Shephard, N.G., Harvey, A.C., 1990. On the probability of estimating a deterministic  
843 component in the local level model. *J. Time Ser. Anal.* 110 (4), 339–347.
- 844 Silvapulle, M.J., 1992. Robust Wald-type tests of one-sided hypotheses in the linear  
845 model. *J. Am. Stat. Assoc.* 870 (417), 156–161.
- 846 Silvapulle, M.J., Silvapulle, P., 1995. A score test against one-sided alternatives. *J. Am. Stat.*  
847 *Assoc.* 900 (429), 0 342–0 349.
- 848 Smith, S.M., Jenkinson, M., Johansen-Berg, H., Rueckert, D., Nichols, T.E., Mackay, C.E.,  
849 Watkins, K.E., Ciccarelli, O., Cader, M.Z., Matthews, P.M., Behrens, T.E., 2006. Tract-  
850 based spatial statistics: voxelwise analysis of multi-subject diffusion data. *NeuroImage*  
851 310 (4), 1487–1505.
- 852 Stram, D.O., Lee, J.W., 1994. Variance components testing in the longitudinal mixed effects  
853 model. *Biometrics* 500 (4), 1171–1177.
- 854 ter Braak, C.J., 1992. Permutation Versus Bootstrap Significance Tests in Multiple  
855 Regression and ANOVA, volume 376 of *Lecture Notes in Economics and Mathematical*  
856 *Systems*. Springer, Berlin Heidelberg.
- 857 Verbeke, G., Molenberghs, G., 2003. The use of score tests for inference on variance com-  
858 ponents. *Biometrics* 590 (2), 254–262 (0 pp.).
- 859 Verbeke, G., Molenberghs, G., Nov. 2007. What can go wrong with the score test? *Am.*  
860 *Stat.* 610 (4), 0 289–0 290.
- 861 Winkler, A.M., Kochunov, P., Blangero, J., Almasy, L., Zilles, K., Fox, P.T., Duggirala, R.,  
862 Glahn, D.C., 2010. Cortical thickness or grey matter volume? The importance of  
863 selecting the phenotype for imaging genetics studies. *NeuroImage* 530 (3), 0  
864 1135–0 1146.
- 865 Winkler, A.M., Ridgway, G.R., Webster, M.A., Smith, S.M., Nichols, T.E., Feb. 2014. Permu-  
866 tation inference for the general linear model. *NeuroImage (ISSN: 1095-9572)* 92C, 0  
867 381–0 397. <http://dx.doi.org/10.1016/j.neuroimage.2014.01.060>.
- 868 Worsley, K.J., Evans, A.C., Marrett, S., Neelin, P., Nov. 1992. A three-dimensional statistical  
869 analysis for CBF activation studies in human brain. *J. Cereb. Blood Flow Metab.* 120  
870 (6), 0 900–0 918.

UNCORRECTED PROOF